ELSEVIER

Contents lists available at ScienceDirect

International Journal of Production Economics

journal homepage: www.elsevier.com/locate/ijpe



A multi-site production and microgrid planning model for net-zero energy operations



An Pham^a, Tongdan Jin^{a,*}, Clara Novoa^a, Jin Qin^b

^aIngram School of Engineering, Texas State University, San Marcos, TX, 78666, USA ^b School of Management, University of Science and Technology of China, Hefei, 230026, China

ARTICLE INFO

Keywords: Logistics electrification Climate analytics Production planning Microgrid sizing Energy prosumer

ABSTRACT

This paper aims to address two critical questions pertaining to sustainable manufacturing operations. First, how to model and design a multi-facility, production-logistics system under product demand and energy supply uncertainty? Second, is it economically viable to achieve net-zero energy operations through renewable microgrid integration? To answer both questions, we present a joint production scheduling and microgrid sizing model to decarbonize the manufacturing, transportation and warehousing operations by harnessing onsite wind and solar energy. The integrated planning model is solved as a two-stage optimization program: first, scheduling the production to meet the uncertain demand; second, sizing and siting the microgrid systems to meet the electric load of multiple facilities. The preliminary results show that net-zero energy operation is feasible and affordable in locations where the capacity factor of wind and solar generation exceeds 0.25 and 0.45, respectively. Sensitivity analysis shows that battery system combined with solar photovoltaics is cost-effective despite the high capital cost of storage devices. Two managerial insights are also derived. First, integrating onsite renewable power is the ultimate key to realizing net-zero energy industrial operations. Second, grid-connected microgrid generation with net metering results in lower capacity investment than island operation.

1. Introduction

The manufacturing industry is currently undergoing a major transition, with increasing levels of renewable resources being integrated through onsite generation. A net-zero energy production-logistics system is defined as an organization that produces as much renewable energy through onsite generation as it consumes from the utility grid over a year (Pless and Torcellini, 2010). This paper proposes to energize the production, warehousing and transportation facilities with 100 percent of renewable power supplied from distributed energy resources (DER). Typical renewable DER units include wind turbines (WT), solar photovoltaics (PV) and bio-gas fuel cells. Recently, many organizations are striving to attain low carbon industrial operations through DER integration. Anheuser-Busch's Budweiser factory in Fairfield, California installed 3.1 MW wind capacity and 1.2 MW PV arrays on site, providing 40 percent of the green electricity to the factory (Hickey, 2014). OPEX has achieved net-zero use of grid power by installing 2.77 MW roof-top PV in its production-distribution facility (McMahon, 2011). These examples show the manufacturing sector is gearing up for environmental sustainability by directly harnessing onsite renewable energy.

By leveraging microgrid generation, this paper proposes a net-zero energy solution for powering a multi-site, production-logistics system through direct integration of wind- and solar-based DER units. Subject to product demand and energy supply uncertainty, the goal is to jointly optimize the production, inventory, backorders, and the sizing and siting of DER units such that the annualized production-logistics cost including the one from energy is minimized. Sizing and siting are also referred to as DER capacity and location, respectively. Production-inventory models considering various types of uncertainties have been extensively studied in literature. Early studies focus on designing production systems to mitigate the variations in demand, yield, lead time and capacity (Yano and Lee, 1995; Sox and Muckstadt, 1996; Mula et al., 2006). New effort is also made to incorporate emission cap-andtrade and tax policy into the production planning to meet the environmental goal (Gong and Zhou, 2013). Our model also considers the product demand uncertainty, but the main objective is to integrate a wind- and solar-based microgrid system to achieve net-zero energy operation across the entire production-logistics system.

We highlight the contributions of this paper in three aspects. First, our model represents an early attempt to jointly optimize the production planning and the sizing and siting of renewable DER units in a

^{*} Corresponding author. ..

E-mail address: tj17@txstate.edu (T. Jin).

multi-site manufacturing and warehouse system with electrified logistics. In existing literature, the decisions on the production planning and the microgrid sizing are often made separately, which may result in under- or over-capacity allocation of generation capacity. Second, our study expands the supply chain dimensionality by treating energy flow as an endogenous decision variable, along with material, cash and information. This new dimension enables manufacturers to create new values in the production-logistics chain in terms of not only consuming, but also producing energy, i.e. the so-called "energy prosumer". Third, we develop a climate data analytics model to forecast the wind and solar generation based on 64,000 meteorological records across eleven years. This climate analytics approach enables us to transform the stochastic production-logistic planning problem into a two-stage linear optimization model: first, optimizing the production and inventory to satisfy the customer demands; second, sizing and siting the microgrid in each facility to attain the net-zero energy performance goal.

The remainder of the paper is organized as follows. Section 2 reviews existing production-inventory models subject to operational uncertainties and emission criteria. Section 3 describes the working principle of the net-zero energy production-logistics system, and a two-stage planning model is formulated. In Section 4, solution methods based on renewable generation analytics of 11-year meteorological data are elaborated. In Sections 5 and 6, we test the proposed model in eight cities with various climate conditions, and further derive managerial insights. Section 7 concludes the paper.

2. Literature review

Stochastic production-inventory planning models can be broadly classified into two categories according to the aspects they tackle: operational uncertainty and environmental constraint. Studies considering the operational uncertainty aim to address the variations or randomness associated with customer demand, process yield, lead time. production capacity and material supply. Federgruen and Zipkin (1984) design a scholastic production system for a central plant that fulfills the random demands from several locations by minimizing the expected backorders and holding cost. Lee and Yano (1988) propose a back-track dynamic programing method to determine the optimality of a serial production system with the goal to minimize operating, holding, and backorder costs subject to random yield. Higle and Kempf (2010) develop a stochastic production planning model under both material supply and demand uncertainty using Markov decision process. Zhang et al. (2012) investigate a multi-echelon uncapacitated lot-sizing problem where the intermediate echelons face uncertain demands of both internal and external customers. More recently, Megahed and Goetschalckx (2018) optimize a multi-echelon wind turbine supply chain where supplier's random yield, stochastic lead times and backorders are all considered. In general, these models aim to lower the production cost or to satisfy the customer demand by handling a variety of uncertainties arising from material suppliers, in-house processes and downstream customers. Our paper also considers demand uncertainty, but the main objective is to integrate intermittent renewable power into a multi-facility, production-logistics system for attaining net-zero energy operations.

Recently a number of researchers start to model and design low-carbon production-inventory systems based on one of the following strategies: 1) energy conservation or power efficiency; 2) carbon cap-and-trade, and tax programs; and 3) onsite or microgrid generation. The main idea of energy conservation is to increase the machine usage or reduce its idle time so that less power is wasted during the production time. For instance, Choi and Xirouchakis (2014) formulate a linear programing model in an aggregate production environment to minimize a weighted objective function that comprises energy, inventory, and backorders. Similarly, Masmoudi et al. (2017) optimize the lot-sizing problem in each production period for minimizing the cost comprised of electrical, inventory, and set-up expense. Very recently,

Zhang et al. (2018) investigate a sizing problem for a fuel-based distributed generator in a flow shop manufacturing process under critical peak pricing contract. A mixed-integer non-linear programming model is formulated to jointly optimize the generation capacity and the machine on-off strategy such that the sum of the utility and generation cost is minimized.

Emissions cap-and-trade and tax programs are a market-based mechanism designed to control and curb carbon and pollutant generation. For instance, Hua et al. (2011) derive the optimal EOQ order quantity to investigate the impacts of carbon emission trading mechanism on order decisions and total cost. Bouchery et al. (2012) study how firms manage carbon footprints in transportation and warehousing facilities under emission cap-and-trade scheme. Gong and Zhou (2013) investigate a two-technology, production-inventory problem using emissions trade and allowance scheme. Later, Zhang et al. (2016) further extend the model to multi-technology systems.

In a renewable microgrid operation, wind- and solar-based DER units are installed in proximity to the industrial facility for the direct supply of renewable energy. Golpira et al. (2018) and Zhang et al. (2017) redesign the flow shop scheduling models to lower the energy cost and the carbon emissions using grid-connected wind- or solarbased microgrid technology. Pechmann et al. (2016) investigate a virtual power plant comprised of wind, solar, biomass, and energy storage to satisfy the demand of a single manufacturing firm. Jin et al. (2017) propose a linear optimization model to integrate onsite wind and solar power for a multi-site supply chain comprised of three factories, two warehouses and four retailers. The model is developed at the strategic level to identify the sizing and siting of WT and PV units with minimum cost. Golari et al. (2017) integrate distributed wind and solar power along with main grid hydro energy into a multi-site, multi-stage production system to meet the green energy coefficient criterion. Assuming product demand is deterministic, their model jointly schedules the production and renewable energy supply such that the cost of the entire planning horizon is minimized.

This paper aims to size and site renewable microgrids in a multi-site, production-logistics system for attaining the net-zero energy performance goal. Our approach differs from energy conservation and carbon cap-and-trade and tax in that wind- and solar-based microgrid technologies transform the traditional manufacturers from an energy user to an energy prosumer who not only consumes the electricity, but also produces green energy. Along this line, this paper extends the work of Jin et al. (2017) and Golari et al. (2017) in two aspects. First, we relax the deterministic demand assumption and the product demand is treated as a random quantity, which is more realistic. Second, a climate data analytics method is developed to characterize the intermittency of wind and solar generation. This enables the original stochastic mixedinteger programming model to be converted into a two-stage deterministic optimization, significantly reducing the computational load.

3. Model Setting

3.1. A production-logistics system with microgrid generation

Fig. 1 depicts a production-logistics system comprised of *K* factories and one central warehouse. Finished goods are shipped from factories to the warehouse using electric trucks (e-trucks). The energy required to perform all necessary operations are jointly supplied by wind- and solar-based microgrid systems installed adjacent to the local facilities. Renewable energy is also used to charge the batteries of e-trucks before departing from the facilities. Charging stations are available on route to recharge the batteries if the travel distance is larger than the battery range. Our goal is to create a net-zero energy zone across manufacturing, transportation, and warehouse facilities.

Since the wind speed and the weather conditions are stochastic, the output of the microgrid system at a random point in time may be higher or lower than the facility's load. If power shortage occurs, electricity is

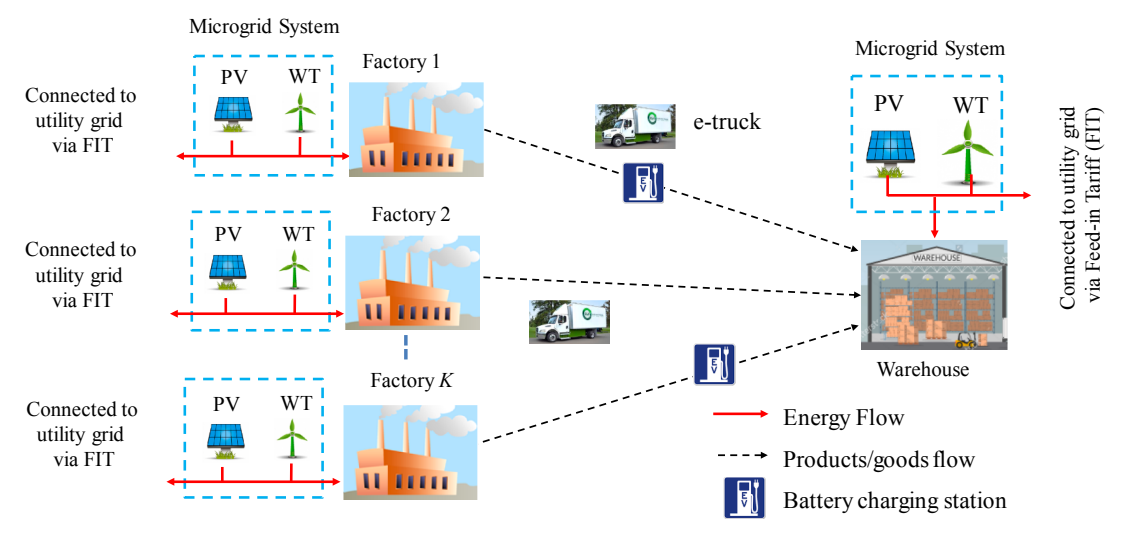


Fig. 1. A multi-site, production-logistics system with microgrid generation.

imported from the main grid to meet the load. To achieve the net-zero energy performance, this "borrowed" electricity must be "returned" later on. This can be realized in the days when wind blows hard or the sun radiation is strong. The surplus energy from the microgrid is returned to the main grid under feed-in tariff or net metering policies (Hu et al., 2015). This paper also considers an island microgrid system that is physically disconnected from the main grid. The model notation is listed in Table 1 .

3.2. A stochastic planning model for net-zero energy operation

We investigate a multi-site, production-logistics system comprised of K factories and N warehouses. As shown in Fig. 1, each factory is able to produce I product types, and finished goods are shipped to the warehouses via e-trucks. The goal is to optimize the production, inventory, and backorders in each period to meet the uncertain demands. To achieve net-zero energy operation, we further allocate renewable DER units at each site to meet the power demand of the entire system. The model objective function is to minimize the total cost comprised of production, logistics and energy generation. Denoted as Model P1, this integrated production and microgrid planning model is formulated as

Model P1:

Minimize:

$$f(\mathbf{x}, \mathbf{y}, \mathbf{z}, \mathbf{P}^{c}) = \sum_{i=1}^{I} \sum_{j=1}^{J} \sum_{k=1}^{K} \sum_{n=1}^{N} (p_{ijk} + \pi_{ikn}) x_{ijkn}$$

$$+ \sum_{i=1}^{I} \sum_{j=1}^{J} \sum_{n=1}^{N} h_{ijn} y_{ijn} + \sum_{i=1}^{I} \sum_{j=1}^{J-1} \sum_{n=1}^{N} b_{ijn} z_{ijn}$$

$$+ \sum_{g=1}^{G} \sum_{k=1}^{K} \phi_{g} a_{g} P_{gk}^{c}$$

$$+ E_{\zeta} \sum_{j=1}^{J} \sum_{g=1}^{G} \sum_{k=1}^{K} \tau_{gk} P_{jgk} (\zeta) (b_{g} - c_{g})$$

$$+ \sum_{g=1}^{G} \sum_{n=1}^{N} \phi_{g} a_{g} P_{gn}^{c}$$

$$+ E_{\zeta} \sum_{j=1}^{J} \sum_{g=1}^{G} \sum_{n=1}^{N} \tau_{gn} P_{jgn} (\zeta) (b_{g} - c_{g})$$

$$(1)$$

Subject to:

$$\Pr\left\{\sum_{k=1}^{K} x_{i1kn} + y_{i0n} - y_{i1n} + z_{i1n} < D_{i1n}\right\} \le 1 - \gamma; j = 1, \forall i, \forall n$$
(2)

$$\Pr\left\{\sum_{k=1}^{K} x_{ijkn} + y_{ij-1n} - y_{ijn} - z_{ij-1n} + z_{ijn} < D_{ijn}\right\} \le 1 - \gamma; \ j = 2, 3, ..., J - 1, \forall i, \forall n$$
(3)

$$\Pr\left\{\sum_{k=1}^{K} x_{iJkn} + y_{iJ-1n} - y_{iJn} - z_{iJ-1n} < D_{iJn}\right\} \le 1 - \gamma; j = J, \forall i, \forall n$$
(4)

$$\sum_{i=1}^{I} \sum_{n=1}^{N} v_{ikr} x_{ijkn} \le w_{jkr} \; ; \; \forall \; j \; , \forall \; r \; , \forall \; k$$

$$\tag{5}$$

$$\sum_{i=1}^{J} \sum_{j=1}^{J} \sum_{n=1}^{N} (e_{ik} + q_{\nu} d_{kn} m_i) x_{ijkn} + \sum_{n=1}^{N} q_{\nu} n_{kn} d_{kn} w_{\nu} = E_{\zeta} \sum_{j=1}^{J} \sum_{g=1}^{G} \tau_{gk} P_{jgk}(\zeta); \forall k$$
(6)

$$t_{w}L_{n} + \sum_{k=1}^{K} q_{v} n_{kn} d_{kn} w_{v} = E_{\zeta} \sum_{j=1}^{J} \sum_{g=1}^{G} \tau_{gn} P_{jgn}(\zeta); \forall n$$
(7)

$$y_{i0n} = 0$$
; for $\forall i, \forall n$ (8)

$$P_{gk}^c \ge 0 \; ; \forall \; g \; , \forall \; k \tag{9}$$

$$P_{gn}^c \ge 0$$
; for $\forall g$, $\forall n$ (10)

$$x_{ijkn}, y_{ijn}, z_{ijn} \ge 0$$
, integer (11)

Model P1 is a mixed-integer stochastic programming problem because it involves uncertain product demand D_{ij} and variable power $P_{gk}(\zeta)$. Note that \mathbf{x} , \mathbf{y} , \mathbf{z} and $\mathbf{P^c}$ are the decision variables. Particularly \mathbf{x} , \mathbf{y} , and \mathbf{z} represent the production, inventory, and backorders in each period. $\mathbf{P^c}$ represents the capacity or sizing of WT and PV in each facility. Objective function (1)) calculates the total system cost comprised of manufacturing, transportation, warehousing and energy consumption. The fourth term is the annualized microgrid equipment cost. Note that $\phi_g = (i_e(1+i_e)^{n_e})/((1+i_e)^{n_e}-1)$ is the capital recovery factor of generating technology g, where n_e is the number of years of paying off the loan, and i_e is the annual discount rate. The last term is the expected cost associated with maintenance & operations, and carbon credits that depend on the output power $P_{igk}(\zeta)$ in period j.

Model P1 involves ten types of constraints. Constraints (2) to (4) are the production-demand balance equations represented by chance constraints, and γ is the probability of meeting the demand. No backorders are allowed in the initial and last periods, hence $z_{i0n}=0$, and $z_{iJn}=0$. Constraint (5) indicates that the resource r used to make product i in period j at factory k is confined to the availability. Constraint(6) is the renewable energy balance equation, stating that the annual electricity consumed by factory k and the forward logistics is fully offset by onsite renewable energy, hence attaining the net-zero energy performance. Similarly, constraint (7) defines the energy balance of the warehouse, stating that the total warehousing energy including the reverse

Table 1
Notation and decision variables.

Notation	Definition
I	number of product types, $i = 1, 2,, I$
J	number of production period, $j = 1, 2,, J$
K	number of factories, $k = 1, 2,, K$
N	number of warehouses, $n = 1, 2,, N$
G	number of renewable generation technologies, $g=1,\ 2,\ G$
R	number of resources required in the production, $r = 1, 2,, R$
Pijk	cost of making one unit of product i in period j in factory k (\$/item)
h_{ijn}	unit holding cost of product i in period j in warehouse n (\$/item/period)
b_{ijn}	unit backorder cost of product i in period j in warehouse n (\$/item)
π_{ikn}	cost of shipping one unit of product i from factory k to warehouse n (\$/item)
$ u_{ikr}$	resource r consumed for making one unit of product i in factory k
w_{jkr}	available amount of resource r in period j in factory k
q_{ν}	electric vehicle energy intensity rate (MWh/kg/km)
w_{ν}	vehicle self-weight (kg)
d_{kn}	distance between factory k and warehouse n (km)
m_i	unit weight of product type i (kg/item)
D_{ijn}	random demand for product i in period j from warehouse n
μ_{ijn}	mean demand of D_{ijn}
σ_{ijn}	standard deviation of D_{ijn}
n_{kn}	number of yearly trips between factory k and warehouse n
t_w	number of operating hours of the warehouse (hours) number of generation hours of technology g per period in
$ au_{gk}$	factory <i>k</i> number of generation hours of technology <i>g</i> per period in
$ au_{gn}$	warehouse n
a_g a_b	capacity cost for generation technology g (\$/MW) capacity cost for battery storage system (\$/MWh)
b_g	operation and maintenance cost for generation technology g (\$/MWh)
c_g	carbon credits for generation technology <i>g</i> (\$/MWh)
e_{ik}	energy consumed for producing one unit of product i in factory k (MWh/item)
L_n	electricity demand (load) in warehouse n (MW)
γ	probability of meeting the product demand
ϕ_{g}	capital recovery factor of renewable generation technology
ϕ_b	capital recovery factor of battery storage system b
v_c, v_r, v_s	cut-in, rated and cut-off wind speed, respectively random wind profile and weather conditions in a period
ζ $P_{jgk}(\zeta)$	random power output of generation technology <i>g</i> in factory <i>k</i> and period <i>j</i>
$P_{jgn}(\zeta)$	random power output of generation technology g in warehouse n and period j
$\lambda_{gk}(\zeta)$	capacity factor of generation technology g in factory k
$\lambda_{gn}(\zeta)$	capacity factor of generation technology g in varehouse n
E_{ζ}	expectation operator with respect to ζ
B^{s}_{jk}	energy stored in the battery in period j at factory k
B_{jn}^{s}	energy stored in the battery in period j at warehouse n
Decision Variables	Definition
x_{ijkn}	quantity of product i produced in period j in factory k shippedto warehouse n
y_{ijn}	inventory of product i in period j in warehouse n
z_{ijn}	backorder of product i in period j in warehouse n
P_{gk}^c	power capacity of generator g in factory k (unit: MW)
P_{gn}^c	power capacity of generator <i>g</i> in warehouse <i>n</i> (unit: MW)
B_k^c	battery storage capacity in factory <i>k</i> (unit: MWh)
$B_n^{\ c}$	battery storage capacity in warehouse n (unit: MWh)

transportation is fully offset by the onsite renewable generation in a year. It is worth mentioning that net-zero energy does not mean that the output of WT and PV always equals the instantaneous electricity load; rather it means the aggregate renewable generation during the course of a year equals the total energy use of a facility including e-trucks. Constraints (6) and (7) are also applicable to the situations where the e-truck recharges its battery from external charge stations when the trip is

beyond its drive range. Constraint (8) states that there is no initial inventory at the beginning of production. Constraints (9)-(11) simply define the non-negativity of the decision variables.

3.3. A two-stage optimization model

Further analysis shows that Model P1 can be decomposed and solved in two stages. In stage 1, we optimize the production, inventory and the backorders in each period to minimize the total non-energy costs $f_1(\mathbf{x}, \mathbf{y}, \mathbf{z})$. In stage 2, we further allocate the capacity of WT and PV at each site to meet the electricity needs of factories and warehouses and minimize the total cost $f_2(\mathbf{P^c}; \mathbf{x}, \mathbf{y}, \mathbf{z})$ subject to net-zero energy requirement. Now P1 is transformed into a two-stage optimization model, denoted as P2, as follows

Model P2-1:

$$f_{1}(\mathbf{x}, \mathbf{y}, \mathbf{z}) = \sum_{i=1}^{I} \sum_{j=1}^{J} \sum_{k=1}^{K} \sum_{n=1}^{N} (p_{ijk} + \pi_{ikn}) x_{ijkn} + \sum_{i=1}^{I} \sum_{j=1}^{J} \sum_{n=1}^{N} h_{ijn} y_{ijn}$$

$$+ \sum_{i=1}^{I} \sum_{j=1}^{J-1} \sum_{n=1}^{N} b_{ijn} z_{ijn}$$

$$(12)$$

Subject to:

$$\sum_{k=1}^{K} x_{i1kn} + y_{i0n} - y_{i1n} + z_{i1n} \ge \mu_{D_{i1n}} + Z_{\gamma} \sigma_{D_{i1n}}; \text{ for } j = 1, \forall i \text{ and } \forall n$$
(13)

$$\sum_{k=1}^{K} x_{ijkn} + y_{ij-1n} - y_{ijn} - z_{ij-1n} + z_{ijn} \ge \mu_{D_{ijn}} + Z\sigma_{D_{ijn}}; \ j = 2, 3, ..., J-1, \forall i, \forall n$$
(14)

$$\sum_{k=1}^{K} x_{iJkn} + y_{iJ-1n} - y_{iJn} - z_{iJ-1n} \ge \mu_{DiJn} + Z_{\gamma} \sigma_{DiJn}; j = J, \forall i, \forall n$$
(15)

$$\sum_{i=1}^{I} \sum_{n=1}^{N} v_{ikr} x_{ijkn} \le w_{jkr} ; \forall j, \forall r, \forall k$$

$$\tag{16}$$

$$y_{i0n} = 0 \; ; \forall \; i, \; \forall \; n \tag{17}$$

$$x_{ijkn}, y_{ijn}, z_{ijn} \ge 0$$
, integer (18)

Model P2-2

$$f_{2}(\mathbf{P}^{c}; \mathbf{x}, \mathbf{y}, \mathbf{z}) = \sum_{g=1}^{G} \sum_{k=1}^{K} \phi_{g} a_{g} P_{gk}^{c}$$

$$+ E_{\zeta} \sum_{j=1}^{J} \sum_{g=1}^{G} \sum_{k=1}^{K} \tau_{gk} \lambda_{jgk}(\zeta) P_{gk}^{c}(b_{g} - c_{g})$$

$$+ \sum_{g=1}^{G} \sum_{n=1}^{N} \phi_{g} a_{g} P_{gn}^{c}$$

$$+ E_{\zeta} \sum_{j=1}^{J} \sum_{g=1}^{G} \sum_{n=1}^{N} \tau_{gn} \lambda_{jgn}(\zeta) P_{gn}^{c}(b_{g} - c_{g}) + f_{1}(\mathbf{x}, \mathbf{y}, \mathbf{z})$$

$$(19)$$

Subject to:

$$\sum_{i=1}^{J} \sum_{j=1}^{J} \sum_{n=1}^{N} (e_{ik} + q_{v} d_{kn} m_{i}) x_{ijkn} + \sum_{n=1}^{N} q_{v} n_{kn} d_{kn} w_{v}$$

$$= E_{\zeta} \sum_{j=1}^{J} \sum_{g=1}^{G} \tau_{gk} \lambda_{jgk} (\zeta) P_{gk}^{c}; \forall k$$
(20)

$$t_{w}L_{n} + \sum_{k=1}^{K} q_{v} n_{kn} d_{kn} w_{v} = E_{\zeta} \sum_{j=1}^{J} \sum_{g=1}^{G} \tau_{gn} \lambda_{jgn}(\zeta) P_{gn}^{c}; \forall n$$
(21)

$$P_{gk}^c \ge 0 \; ; \forall \; g, \; \forall \; k \tag{22}$$

$$P_{gn}^c \ge 0 \; ; \; \forall \; g, \; \forall \; n \tag{23}$$

Since P2-1 is a linear integer program, it can be solved using off-theshelf optimization software. To make the original stochastic optimization model tractable, we convert the chance constraints (2)-(4) into their deterministic counterparts as shown in constraints (13)-(15) where D_{ijn} is assumed to be normally distributed with N (μ_{ijn} , σ_{ijn}^2). In addition, Z_{γ} is the Z-value of the standard normal distribution with probability γ .

Model P2-2 is a linear stochastic optimization model featured with the random capacity factor $\lambda_{igk}(\zeta)$ which is the power generated by generation technology g at a factory k in period j divided by the DER capacity. For instance, if a WT capacity is 2 MW, and the actual output in a particular day is only 0.8 MW due to small wind, the capacity factor is 0.8/2 = 0.4. In other words, $P_{jgk}(\zeta)$ relates to P_{gk}^c by $P_{jgk}(\zeta) = \lambda_{jgk}(\zeta)$ P_{gk}^c for $0 \le \lambda_{jgk}(\zeta) \le 1$. Similar connection can be made for $P_{gn}^c(\zeta)$ with $P_{jgn}(\zeta) = \lambda_{jgn}(\zeta)P_{gn}^c$ for $0 \le \lambda_{jgn}(\zeta) \le 1$. We propose a Renewable Integration Analytics (RIA) method to characterize $\lambda_{jgk}(\zeta)$ and $\lambda_{jgn}(\zeta)$ by taking into account stochastic climate conditions in each facility. Specifically, RIA leverages large amounts of meteorological data, such as multi-year wind speed and weather information in a region, to predict the future renewable generation. The estimated capacity factors are then fed into P2-2 so that the stochastic optimization model is transformed into a deterministic counterpart. Fig. 2 shows how RIA is performed on WT and solar PV systems at each site, and the resulting data are merged with P2-1 to size and site WT and PV units in the second stage.

4. Renewable Integration Analytics

4.1. Pooling climate data

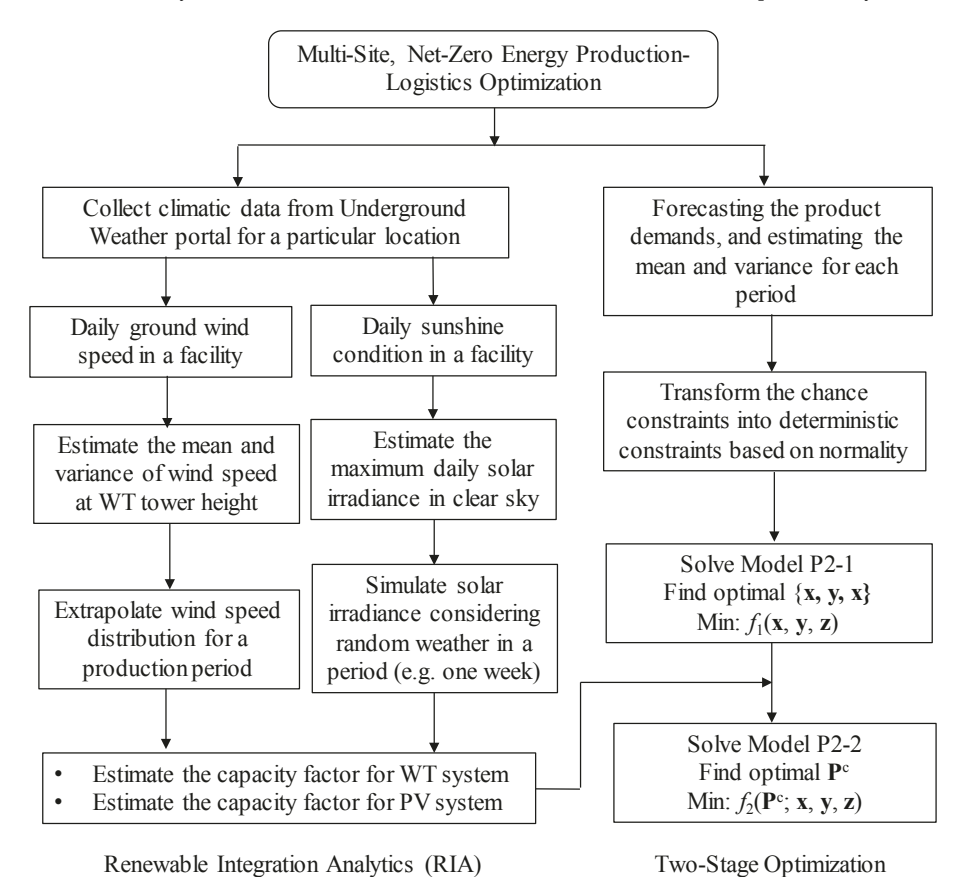
We use 11-year climate data to investigate the feasibility of attaining net-zero energy production-logistics operations through renewable microgrid generation. Eight cities in different areas of the world are selected to test Model P2. The latitude (degree), average wind speed and weather conditions of each city are summarized in Table 2.

Note that Wellington and Christchurch are located in the Southern Hemisphere, and the other cities are in the Northern Hemisphere. The daily wind speed and the weather conditions of these cities are retrieved from the Weather Underground portal (WU, 2017). The weather conditions are classified into nine states, namely, clear day, scattered cloud (SC), partially cloudy (PC), mostly cloudy (MC), overcast, rain, fog, storm (including T-storm) and snow.

For each city, daily wind speed and weather conditions over eleven years from 2006 to 2016 are collected to obtain accurate estimations of climate conditions. A total of 4015 daily wind speed measurements are collected for each city, and a total of 32,120 wind speed samples are used to estimate the WT capacity factors for eight cities. Similarly, the daily weather conditions (i.e. sunshine) for each city are also obtained from UW portal with 4015 data points for eleven years. A total of $4015 \times 8 = 32,120$ records are collected for eight cities over eleven years. By aggregating the wind and weather information, the size of the dataset for RIA reaches $32,120 \times 2 = 64,240$. As shown in Table 2, Wellington has a strong wind profile with AWS of 6.71 m/s, but only six clear days per annum. Luxor has an extremely strong sunshine with 337 clear days, but the AWS is only 1.44 m/s. San Francisco has a medium wind profile of 4.05 m/s, and the number of days with sunshine and scattered cloud reaches 123 per annum. The climate conditions of these cities are relatively diverse, representing the areas where the human beings choose to live. Below the RIA method is applied to the 11-year data pool to analyze the wind and solar generation.

4.2. Estimating wind capacity factor

Wind speed data shown in Table 3 is usually recorded by the Automated Surface Observing Systems (ASOS) of the local airport. These ASOS wind sensors are typically installed 8–10 m above the ground (WU, 2017). Due to "no-slip" boundary condition, the frictional drag of



 $\textbf{Fig. 2.} \ \, \textbf{Integration of RIA with two-stage optimization.} \\$

Table 2
Average wind speed and weather conditions between 2006 and 2016.

Country	New Zealand		Egypt		USA			
City	Wellington	Christchurch	Aswan	Luxor	Yuma	San Francisco	El Paso	Phoenix
Latitude (deg)	41.3	43.5	24.1	25.7	32.7	37.8	31.8	33.5
Ground AWS	6.71	3.84	7.93	1.44	2.97	4.05	3.76	2.80
Ground SWS	2.91	1.77	2.29	0.67	1.40	1.83	1.78	1.05
Clear days	6	20	356	337	165	28	64	65
SC	68	41	5	11	109	95	111	115
PC	109	98	3	14	65	136	108	133
MC	5	11	0	0	0	13	5	4
Overcast	1	3	0	1	0	2	1	1
Rain	170	131	0	1	13	65	31	25
Fog	2	56	0	0	1	24	2	0
Storm	3	3	0	0	11	3	41	22
Snow	0	3	0	0	0	0	0	0

Note: AWS = average wind speed (m/s), SWS = standard deviation of wind speed (m/s).

the ground surface causes the wind speed to be zero, while the air pressure gradient causes the wind speed to increase with the height (Letchford and Zachry, 2009). Let v_g (m/s) be the wind speed measured near the ground at height h_g . According to Heier (2005), the wind speed at the height h can be estimated by

$$v_h = v_g \left(\frac{h}{h_g}\right)^{\kappa}$$
; for $h \ge h_g$ (24)

where parameter " κ " is the Hellman exponent that depends on the coastal location, the shape of the terrain, and the stability of the air. A value between 0.27 and 0.34 is often assumed for κ in the human inhabited areas (Blackadar and Tennekes, 1968; Heier, 2005). For instance, if $\kappa = 0.34$, the wind speed at h = 80 m would be $\nu_h = \nu_g$ (80/10)^{0.34} = 2.03 ν_e , twice of the wind speed near the ground.

Capacity factor (CF) is defined as the average power generated divided by the rated power capacity. It is an important index to measure the energy throughput of intermittent generators like WT and PV. Without loss of generality, we use the wind speed data of the first week in Wellington to illustrate the procedure of calculating the CF of WT. Rows 2–7 in Table 3 are the daily ground wind speed in Week 1 between 2006 and 2016. Assuming $\kappa=0.27$, the corresponding wind speed at 80-m height is obtained using Equation (Li et al., 2017), and the results are given in table as well. A height of $h=80\,\mathrm{m}$ is assumed because this is the typical tower height for commercial WT with capacity of 1.5–3 MW.

The two-parameter Weibull distribution is perhaps the most popular wind distribution model because it is capable of fitting wind profiles in most areas of the world (Vallee et al., 2007; Weekes and Tomlin, 2014). The probability density function is shown in Equation (A2). The wind speed data at 80-m tower in Table 3 fits the Weibull distribution with

c=15.31 m/s and k=3.33 at 95% confidence level, where c and k are the Weibull scale and shape parameters, respectively. Finally, we estimate the wind CF for Week 1 using Equation (A4), resulting in $\lambda_w=0.80$. The CF is obtained based on $\nu_c=3$ m/s, $\nu_r=12$ m/s and $\nu_s=25$ m/s. These are the typical characteristic wind speeds of commercial WT systems (Karki et al., 2006). Fig. 3 plots the weekly CF values that are derived from 32,120 meteorological data of eight cities. The average wind CF in Wellington exceeds 0.6, yet the average CF in Luxor is only 0.05.

4.3. Estimating PV capacity factor

The daily weather conditions retrieved from the WU web portal are classified into nine states as shown in Table A2 in Appendix A. For illustration purposes, Table 4 lists the daily weather state of Week 1 in Wellington from 2006 to 2016. The number of days for a particular state is counted, and the results are summarized in Table 5. For instance, the cumulative number of "Clear" days for Week 1 is three over eleven years, and the cumulative number of "Rain" days is 25. For a given day in that week, the probability of a particular weather state can be estimated. For instance, the probability of a "Clear" day is 3/77 = 0.04, and the probability of "Rain" is 25/77 = 0.32. These values can be used to simulate the PV output for Week 1 in Wellington.

The solar radiation incident on a PV surface at time t, denoted as I_t (W/m²), can be precisely predicted if the sky has no cloud. Detailed procedures to estimate I_t under the clear sky are available in Appendix A. The randomness of PV generation is caused by the uncertain weather conditions. To address the random cloud movement, the weather coefficient W_t is used to adjust the actual I_t . For instance, if it is "Clear", $W_t = 1$, meaning the PV receives 100 percent of I_t . If it is "PC," then only 50 percent of I_t reaches the PV surface. In a snowy day, $W_t = 0$

Table 3 Wind Speed of Week 1 in Wellington (unit: m/s, and $\kappa = 0.27$).

	Day	2016	2015	2014	2013	2012	2011	2010	2009	2008	2007	2006
10-m above ground	1	2.68	5.81	8.49	8.94	7.60	5.36	9.39	8.49	2.68	11.62	3.58
	2	4.02	5.81	8.49	12.52	6.71	8.94	11.62	8.49	7.15	11.62	10.73
	3	7.60	6.26	12.52	9.83	5.36	8.94	8.05	9.83	11.18	8.94	9.83
	4	11.62	6.26	9.39	4.02	6.26	8.05	9.39	4.47	6.26	3.58	10.28
	5	2.68	10.28	8.94	3.58	11.18	5.81	5.36	7.60	4.47	8.94	5.36
	6	4.02	6.71	7.60	5.81	8.05	5.81	10.73	10.73	8.49	12.52	4.47
	7	8.94	4.92	10.28	7.60	6.26	10.73	12.07	11.18	8.94	5.36	7.60
80-m tower height	1	4.70	10.19	14.89	15.68	13.32	9.41	16.46	14.89	4.70	20.38	6.27
	2	7.05	10.19	14.89	21.95	11.76	15.68	20.38	14.89	12.54	20.38	18.81
	3	13.32	10.97	21.95	17.24	9.41	15.68	14.11	17.24	19.59	15.68	17.24
	4	20.38	10.97	16.46	7.05	10.97	14.11	16.46	7.84	10.97	6.27	18.03
	5	4.70	18.03	15.68	6.27	19.59	10.19	9.41	13.32	7.84	15.68	9.41
	6	7.05	11.76	13.32	10.19	14.11	10.19	18.81	18.81	14.89	21.95	7.84
	7	15.68	8.62	18.03	13.32	10.97	18.81	21.16	19.59	15.68	9.41	13.32

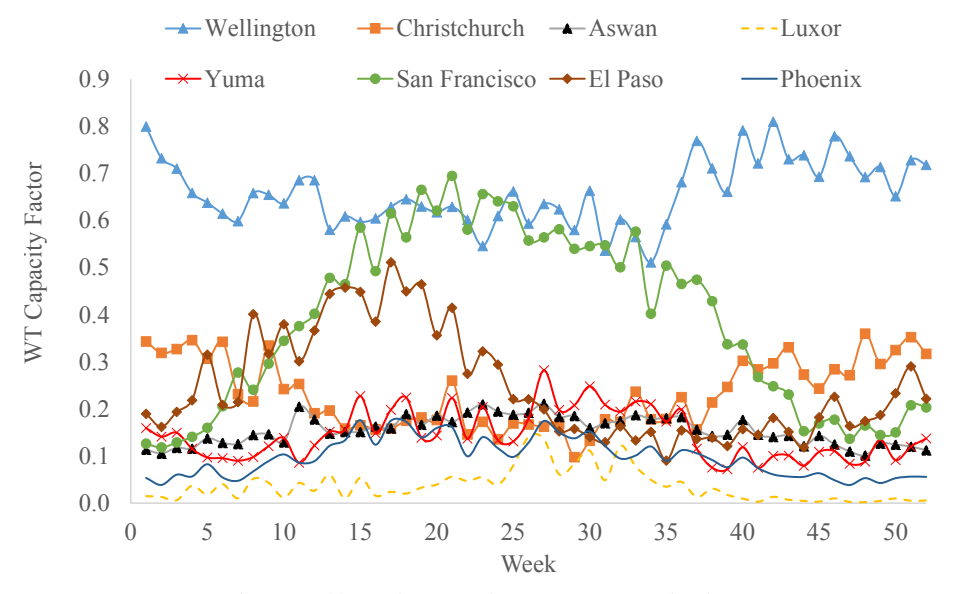


Fig. 3. Weekly wind capacity factor at 80-m tower height.

because the PV surface is likely to be covered by snow. The values of W_t under different weather states are listed in Table A2.

Based on the 3-step PV generation model in Appendix A, we develop a Matlab program to simulate the daily weather state for each city. The PV generation is averaged over a week, and then divided by the PV capacity to obtain the CF in that week. The simulation is repeated over 52 weeks to cover one year. To reduce the simulation variability, the 52-week simulation is repeated over eleven years to obtain the average weekly CF. Fig. 4 plots the weekly CF of PV generation for eight cities. The CF in Aswan and Luxor is above 0.4 on average, while the lowest CF occurs in Wellington and Christchurch with the average CF below 0.15.

4.4. Electric vehicle energy intensity rate

For battery-powered vehicles, the electricity required to move an object from one location to another depends on the weight of the object, the travel distance, and the speed. For example, the battery capacity of a Condor e-truck is 0.05 MWh (or 50 KWh), and the driving range of a fully charged Condor can reach up to 160 km at 100 km/h (EV-Fleet, 2017). The electric vehicle energy intensity rate, denoted as q_v , is defined as the amount of battery energy consumed in order to move 1 kg object across 1 km at a specific speed (e.g. 100 km/h). That is

$$q_{\nu} = \frac{E_{EV}}{m \times d_{\text{max}}},\tag{25}$$

where E_{EV} is the battery capacity in MWh, $d_{\rm max}$ is the driving range at speed ν measured in km and m is the vehicle gross weight including the payload. For instance, the gross weight of a Condor is approximately 2630 kg. At $\nu = 100$ km/h, we obtain q_{100} as follows

Table 5The probabilities of weather states for week 1 in wellington.

Day	Clear	SC	PC	MC	OC	Rain	Fog	Storm	Snow
1	1	4	3	0	0	3	0	0	0
2	0	3	3	0	0	5	0	0	0
3	0	2	3	0	0	6	0	0	0
4	0	4	3	0	0	4	0	0	0
5	2	3	3	0	0	2	1	0	0
6	0	0	7	1	0	3	0	0	0
7	0	0	9	0	0	2	0	0	0
Total	3	16	31	1	0	25	1	0	0
Probability	0.04	0.21	0.40	0.01	0.00	0.32	0.01	0.00	0.00

$$q_{100} = \frac{0.05}{2630 \times 160} = 1.19 \times 10^{-7} \ MWh/kg/km \tag{26} \label{eq:26}$$

Given q_{ν} , we can estimate the energy required to move different weights over an arbitrary distance at a given speed. For instance, to move a 4000-kg object (including vehicle weight) over 100 km at a speed of $100\,\mathrm{km/h}$, the amount of electricity consumed would be $q_{100} \times 4000 \times 100 = 0.04762\,\mathrm{MWh}$. Charging stations along the route are required to "refill" the batteries of e-trucks if the travel distance is larger than the driving range, which is typically 120–160 km for a current e-truck (Daclison-Dickey, 2013).

5. Numerical experiments

5.1. Single factory and warehouse system

We first implement Model P2 in a production-logistics system comprised of one factory and one warehouse. Production data used for this experiment is associated with an electricity-intensive industry that

Table 4Daily weather condition of week 1 from 2006 to 2016 in wellington.

Day	2016	2015	2014	2013	2012	2011	2010	2009	2008	2007	2006
1	Clear	PC	Rain	SC	Rain	PC	SC	SC	SC	Rain	PC
2	Rain	SC	PC	PC	Rain	SC	PC	Rain	SC	Rain	Rain
3	Rain	Rain	Rain	SC	PC	SC	Rain	Rain	PC	PC	Rain
4	Rain	PC	Rain	SC	SC	PC	Rain	SC	PC	SC	Rain
5	Clear	PC	Rain	Clear	PC	Fog	SC	SC	SC	PC	Rain
6	PC	MC	PC	PC	PC	Rain	PC	PC	Rain	PC	Rain
7	PC	Rain	PC	PC	PC	PC	PC	PC	Rain	PC	PC

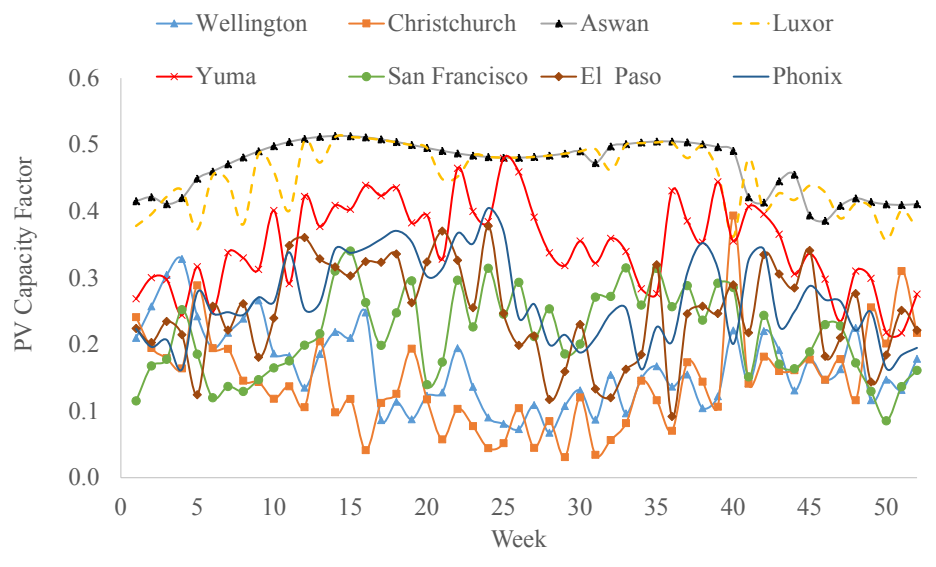


Fig. 4. Weekly solar PV capacity factor of eight cities.

Table 6Parameters for the production-logistics system (exd. = excluding).

Comments	Notation	Product A $(i = 1)$	Product B $(i = 2)$	Unit
Mean demand	μ_{ij}	1000	600	item/period
Standard deviation	σ_{ii}	120	50	item/period
Production cost (exd. energy)	p_i	400	600	\$/item
Holding cost	h_i	20	30	\$/item/period
Backorder cost	b_i	150	250	\$/item/period
Shipping cost (no battery recharge)	π_i	10	15	\$/item
Shipping cost (battery recharge)	π_i	14	19	\$/item
Labor hours	ν_{i1}	16	24	hours/item
Machine hours	v_{i2}	100	200	hours/item
Product weight with package	m_i	3	4	kg/item
Energy consumed	e_i	0.9	1.2	MWh/item

operates 24 h and 7 days a week, such as wafer manufacturing, air separation process, and aluminum refinery. Assume the facility produces two product types, namely A and B. The product demands in each period are uncertain, but follow the normal distribution with known mean and variance. In this experiment, each period corresponds to one week or 168 h, and the planning horizon is 52 weeks. Data associated with product demand, inventory, backorders and transportation are shown in Table 6.

E-trucks are used to ship finished goods from the factory to the warehouse. The weight of the vehicle by itself is $w_{\nu}=5000$ kg, and the electric vehicle energy intensity rate is $q_{\nu}=1.19\times 10^{-7}$ MWh/kg/km at the speed of 100 km/h. The electric load of the warehouse is relatively stable with L=7 MW and the yearly operating time $t_{w}=8760$ h. Round trip frequency between the factory and the warehouse is $n_{kn}=182$ trips/year. Assume the driving range of an e-truck is $d_{\rm max}=150$ km. Two scenarios are considered for estimating the transportation cost:

- If an e-truck can travel from the factory to the warehouse without battery recharge (i.e. $d_{kn} \le d_{max}$), then $\pi_1 = \$10$ /item and $\pi_2 = \$15$ / item for Products A and B, respectively.
- If an e-truck requires the battery recharge because of $d_{kn} > d_{maxo}$ then $\pi_1 = \$14/\text{item}$ and $\pi_2 = \$19/\text{item}$. The higher cost is caused by paying electricity bills and driver's waiting time in the charge stations.

Two critical resources for the production are the labor and machine hours. It is quite difficult to obtain actual availability of labor and machine resources from a real manufacturing industry as these data are considered as confidential information. To closely mimic the reality, we extrapolate the labor and machine hours from a local semiconductor manufacturer in Austin, TX, USA based on their hourly electricity usage. Table B1 presents the available resources over 52 weeks in the factory.

Costs of equipment and operation of WT and PV systems are listed in Table 7. These values are adopted from the works of Freris and Infield (2008) and NREL report (2013). The efficiency of commercial PV varies between 15% and 20% and a conservative $\eta=15\%$ is used in this paper. $T_o=45\,^{\circ}\mathrm{C}$ is the PV operating temperature. To maximize the throughput, PV tilt angle equals the local latitude (i.e. $\beta=\phi$), and it is oriented toward the South (i.e. $\alpha=0$) in the Northern Hemisphere (opposite in the Southern Hemisphere). Lifetime $n_e=20$ years are assumed for WT and PV with $i_e=5\%$ interest rate, thus $\phi_g=0.08024$. Since wind power technology is quite mature now, carbon credits are

Table 7Cost and Operation Parameters of WT and PV systems.

		Symbol	Value	Unit
5×10^6 \$	/A ATAI			UIIIL
	S/MW	a_g	3×10^6	\$/MW
\$			8	\$/MWh
\$	a conservation	-	35	\$MWh
8 h		· ·	84	hour/period
n		-	0.15	N/A
n	n/s	T_o	45	°C
n	n/s	α	0	rad
y	vear	n_e	20	years
			0.05	n/a
8	3 1 1 1 3	\$/MWh hour/period m/s m/s m/s year	S/MWh c_g^s hour/period τ_g m/s η m/s T_o m/s α year n_e	\$/MWh c_g 35 hour/period τ_g 84 m/s η 0.15 m/s T_o 45 m/s α 0 year n_e 20

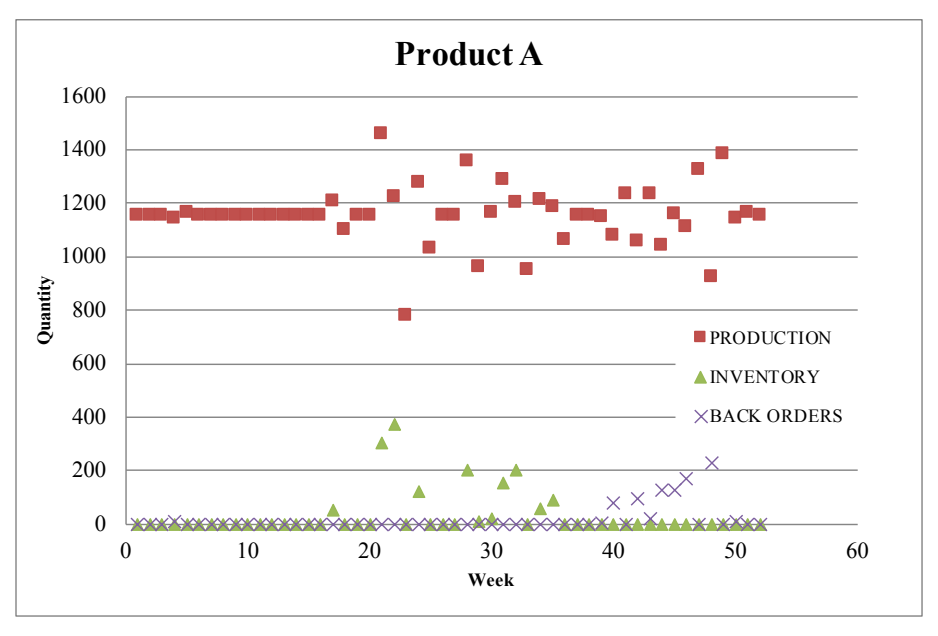


Fig. 5. Production decisions on product A in model P2-1.

only given to PV for offsetting the higher installation cost. For detailed PV generation parameters, please refer to Table A1 in Appendix A.

5.2. Results analysis and comparison

Model P2 is coded using AMPL optimization software containing the CPLEX solver running on an AMD Radeon R6 processor, which runs at 1.8 GHz and contains 4 cores, and 12 GB DRAM. The current model has a total of 316 mixed integer decision variables and more than 210 constraints. Figs. 5 and 6 present the outcome of P2-1 that includes production, inventory, and backorders for Products A and B across 52 weeks at $\gamma = 90\%$ service level.

Variations are observed on weekly production, inventory and backorders for both Products A and B. Take Product A in Fig. 5 as the example. The production is relatively stable in the first 20 weeks, and the variation thereafter is caused by the fluctuation of labor and machine hours. If we compare Fig. 5 with Table B1, from Week 20 the lowest value for the labor hours available reaches 28,867 in Week 23

and 28,497 in Week 38. Similar observations can be found for machine hours. Since the system must meet the demand across 52 weeks, more production will be scheduled when both the labor and the machine hours are abundant like in Weeks 22 and 49. Similarly, backorders are to be higher if the labor and machine hours are lower. In Week 48 the amount of available machine hours is only 226,419, far below the average value of 253,239 h/week.

Next, we solve P2-2 to optimize the sizing and siting of the microgrid considering the production-logistics decisions of P2-1. As shown in Table 8, we investigate three cases by taking into account different climate conditions, namely Wellington and Christchurch (Case 1), Aswan and Luxor (Case 2), and Yuma and San Francisco (Case 3).

Case 1 represents a large wind profile at the factory and the warehouse. We solve P2-2 and the minimum annualized system cost is \$53,797,354 including production, transportation, warehousing and energy generation. Given the carbon credit of \$35/MWh for PV, the model still chooses WT due to the strong wind profile in Wellington and Christchurch. The resulting installed WT capacity is 17.44 MW in the

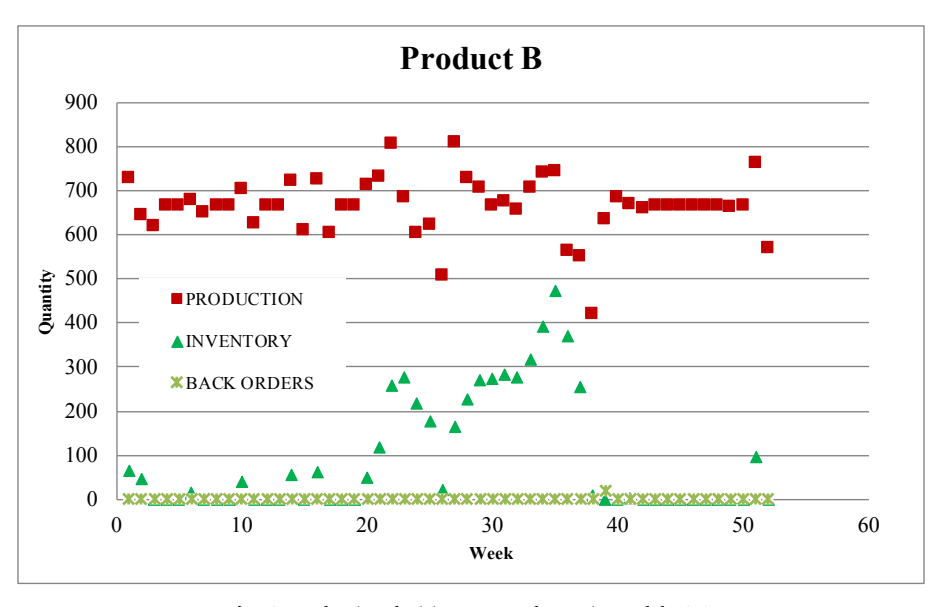


Fig. 6. Production decisions on product B in model P2-1.

Table 8Results of three production-logistics systems.

Case No.	Case 1	Case 2	Case 3
City	Wellington	Aswan	Yuma
Facility	Factory	Factory	Factory
Wind profile	strong wind	Low wind	Medium wind
Weather condition	Weak sun	Strong sun	Strong sun
Generation type	WT	PV	WT
Capacity (MW)	17.44	46.39	75.31
City	Christchurch	Luxor	San Francisco
Facility	Warehouse	Warehouse	Warehouse
Wind profile	Strong wind	Low wind	Strong wind
Weather condition	Weak sun	Strong sun	Medium sun
Generation type	WT	PV	WT
Capacity (MW)	30.07	30.96	18.21
Driving distance (km)	439	238	1051
System cost	\$53,797,354	\$61,139,123	\$59,658,121

factory and 30.07 MW in the warehouse.

In Case 2, Aswan and Luxor have strong sunshine conditions with low wind speed, which is opposite to Case 1. The model chooses to install PV even if its capacity cost is twice of the WT. The installed capacity of PV in the factory is 46.39 MW and the warehouse is 30.96 MW. The annualized system cost is \$61,139,123.

In Case 3, we assume the factory is located in Yuma, AZ with strong sunshine and medium wind, and the warehouse is in San Francisco, CA with strong wind and medium sunshine. Despite the strong sunshine and PV carbon credit, the model chooses WT for Yuma as a more cost-effective solution. The installed WT capacity in the factory is 75.31 MW and in the warehouse is 18.21 MW. The annualized system cost is \$59,658,121.

5.3. Island microgrid operation

Under island operation, the microgrid system is responsible for supplying all the energy to the local facility because of the disconnection from the main grid. Battery storage systems (BSS) can mitigate the power intermittency through energy discharging and charging during peak and off-peak periods. Below we expand Model P2-2 by incorporating BSS into factories and warehouses to realize island microgrid operation. Denoted as P2–2B, the model is given as,

Model P2-2B

Minimize:

$$\begin{split} f_{2B}\left(\mathbf{P^{c}},\,\mathbf{B^{c}};\,\mathbf{x},\,\mathbf{y},\,\mathbf{z}\right) &= \sum_{g=1}^{G} \sum_{k=1}^{K} \phi_{g} \, a_{g} P_{gk}^{c} + \phi_{b} \, a_{b} \sum_{k=1}^{K} B_{k}^{c} \\ &+ E_{\zeta} \sum_{j=1}^{J} \sum_{g=1}^{G} \sum_{k=1}^{K} \tau_{gk} \lambda_{jgk} \left(\zeta\right) P_{gk}^{c} \left(b_{g} - c_{g}\right) \\ &+ \sum_{g=1}^{G} \sum_{n=1}^{N} \phi_{g} \, a_{g} P_{gn}^{c} + \phi_{b} \, a_{b} \sum_{n=1}^{N} B_{n}^{c} \\ &+ E_{\zeta} \sum_{j=1}^{J} \sum_{g=1}^{G} \sum_{n=1}^{N} \tau_{gn} \lambda_{jgn} \left(\zeta\right) P_{gn}^{c} \left(b_{g} - c_{g}\right) \\ &+ f_{1}(\mathbf{x},\,\mathbf{y},\,\mathbf{z}) \end{split}$$

Subject to:

$$\sum_{i=1}^{I} \sum_{n=1}^{N} (e_{ik} + q_{\nu} d_{kn} m_{i}) x_{ijkn} + \sum_{n=1}^{N} q_{\nu} \hat{n}_{kn} d_{kn} w_{\nu} + B_{jk}^{s} - B_{j-1k}^{s}$$

$$\leq E_{\zeta} \sum_{g=1}^{G} \tau_{gk} \lambda_{jgk}(\zeta) P_{gk}^{c}; \forall j, \forall k$$
(28)

$$\hat{t}_{w}L_{n} + \sum_{k=1}^{K} q_{v}\hat{n}_{kn}d_{kn}w_{v} + B_{jn}^{s} - B_{j-1,n}^{s} = E_{\zeta} \sum_{g=1}^{G} \tau_{gn}\lambda_{jgn}(\zeta)P_{gn}^{c}; \forall j, \forall n$$
(29)

$$0 \le B_{jk}^s \le B_k^c \; ; \forall j \; , \forall k$$
 (30)

$$0 \le B_{jn}^s \le B_n^c \; ; \; \forall \; j \; , \; \forall \; n \tag{31}$$

$$B_{0k}^{s} = B_{1k}^{s} = 0 \; ; \; \forall \; k \tag{32}$$

$$B_{0n}^{s} = B_{In}^{s} = 0 \; ; \; \forall \; n \tag{33}$$

In Model P2-2B, B_k^c and B_n^c are the new decision variables representing the BSS capacity in the factory and warehouse, respectively. Objective function (27) minimizes the annualized system cost including the BSS cost. Note that $\phi_b = 0.1295$ is assumed because the lifetime of BSS is typically ten years, and the current cost for a commercial BSS is around \$0.5M/MWh (Hart and Sarkissian, 2016). Constraints (28) and (29) make sure that the energy consumed per period in each facility is fully supplied by the microgrid under island operation. Since these constraints are stated in a period, thus $\hat{t}_w = 168 \, \text{h/period}$ and $\hat{n}_{kn} = 3.5$ trips/period. Constraints (30) and (31) state that the energy stored per period should not exceed the BSS capacity. Constraints (32) and (33) indicate that the BSS energy in the initial and end production period is zero. In Case 4 we use the same input data from Case 1 to solve P2-2B by varying the BSS capacity cost from \$0.5M/MWh to \$0.01M/MWh. Similarly, Case 5 is obtained by using the input data of Case 2. The results of both cases are shown in Figs. 7 and 8.

Two observations can be made from Cases 4 and 5. First, island microgrid operation requires more generation capacity than grid-connected microgrid in order to meet the same facility load. Case 4 shows that the WT capacity in Wellington reaches 21.9 MW, and 64.7 MW in Christchurch without BSS, while under grid-connected operation in Case 1, these capacities are only 17.44 MW and 30.07 MW, respectively. Similar observation can be made in Case 5 as opposed to Case 2 in Aswan and Luxor. Second, BSS with price at \$0.1–0.5M/MWh is not competitive in cities with strong wind. In these locations, the facilities opt to install more WT capacity instead of using BSS to balance the power shortage. However, Case 5 shows that BSS is more attractive to PV systems, and the main reason is because PV installation cost is much higher than WT.

6. Multi-factory and warehouse system

6.1. System settings

Now we implement Model P2 in a two-factory and one-warehouse system with grid-connected microgrid generation. In Case 6, Yuma and El Paso are selected as the factory sites, and Phoenix is the warehouse site. In Case 7, San Francisco and Dallas are the sites for the factory, and Austin is the site of the warehouse. The travel distance between factories and the warehouse is shown in Table 9. The travel frequency between the two factories and the warehouse is $n_{kn} = 186$ trips/year. We adopt the same aggregate demand data in Table 6 to solve Cases 6 and 7. Parameters of WT and PV are given in Table 7. Labor and

Case 4 for Island Operation in Wellington (WL) and Christchurch (CC)

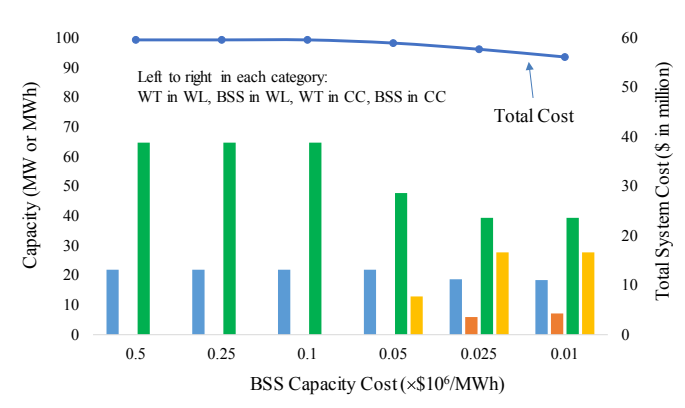


Fig. 7. Microgrid capacity for Case 4 under island operation.



Fig. 8. Microgrid capacity for Case 5 under island operation.

machine hours available for each factory are listed in Table B2 of Appendix B. The average electricity load of each warehouse is $L_n = 7 \text{ MW}$.

6.2. Results analysis and comparison

For Case 6, we first solve model P2-1 at $\gamma=90\%$ service level, and the results of the production-inventory decisions are used as the input data for P2-2 to optimize the microgrid capacity in Yuma, El Paso and Phoenix. For Case 7, based on the result of P2-1, we solve model P2-2 in which San Francisco and Dallas are factories, and Austin is the warehouse location. The sizing and siting of microgrid for Cases 6 and 7 are summarized in Table 10. These results are obtained assuming that the installation cost for WT is \$1.5M/MW for PV is \$3M/MW, and the carbon credit for PV is \$35/MWh. The results of both cases indicate that, despite the strong sunshine in Phoenix and San Francisco and the favorable PV carbon credit, WT is a preferred onsite power source. Similar observations can be made in other locations where WT is more cost-effective than PV regardless of strong sunshine in these sites.

6.3. Sensitivity analysis on levelized cost of energy

Finally we compute the levelized cost of energy (LCOE) of a microgrid system to determine which location is cost-effective in either grid-connected or island operation mode. LCOE is the net present value of the unit-cost of electricity over the lifetime of a particular generating asset. Bolinger et al. (2015) studied the contractual price of renewable power purchase programs between 2008 and 2015 and found that price varies between \$50/MWh and \$120/MWh. Hence \$120/MWh is taken as the reference cost for comparing the LCOE of microgrid.

Table 11 summarizes the LCOE for the studied cases. In grid-connected mode, except Phoenix, all other locations are cost-effective in harnessing microgrid power because their LCOE is below \$120/MWh. In fact, wind generation is particularly appealing if the capacity factor is above 0.23, making the LCOE as low as \$68.8/MWh (see Christchurch in Case 1). In island operation, Wellington and Aswan realize cost-effective operation because their LCOE is below \$120/MWh. Note the LCOE in island operation is estimated assuming BSS cost is \$0.01M/MWh. If BSS is \$0.5M/MWh, only Wellington's LCOE is still below

Table 10Results for multi-factory, one-warehouse systems for Cases 6 and 7.

Case 6			Case 7		
Factory 1 (Yuma)	WT	43.8 MW	Factory 1 (San Francisco)	WT	11.9 MW
Factory 2 (El Paso)	WT	18.56 MW	Factory 2 (Dallas)	WT	16.67 MW
Warehouse (Phoenix)	WT	72.41 MW	Warehouse (Austin)	WT	21.32 MW
Annualized cost	\$61,	243,500	Annualized cost	\$58,	342,352

Table 11Levelized Cost of Microgrid Systems (Note: CF reported is the average value, and GC=Grid Connected).

Case	City	LCOE (\$/MWh)	Generation Type	WT CF	PV CF	Operation Mode
1	Wellington	30.5	WT	0.66	0.16	GC
	Christchurch	68.8	WT	0.23	0.14	GC
2	Aswan	90.1	PV	0.15	0.47	GC
	Luxor	92.4	PV	0.04	0.45	GC
3	Yuma	104.2	WT	0.15	0.35	GC
	San Francisco	46.1	WT	0.39	0.22	GC
4	Wellington	40.2	WT	0.66	0.16	Island
	Christchurch	126.3	WT	0.23	0.14	Island
5	Aswan	108.8	PV	0.15	0.47	Island
	Luxor	181.2	PV	0.04	0.45	Island
6	Yuma	105.2	WT	0.15	0.35	GC
	El Paso	66.4	WT	0.25	0.25	GC
	Phoenix	152.1	WT	0.10	0.27	GC
7	San Francisco	46.1	WT	0.39	0.22	GC
	Dallas	56.7	WT	0.34	0.25	GC
	Austin	65.2	WT	0.27	0.31	GC

\$120/MWh.

7. Conclusions

In this paper a joint production and microgrid planning model is proposed to decarbonize the manufacturing, transportation and warehousing operations under product demand and energy supply uncertainty. Renewables integration analytics is shown to be an effective approach to characterize the intermittent wind and solar generation. The model is solved as a two-stage decision-making process. First, we schedule the production to meet the uncertain demands. Then we size and site the wind, solar and battery units to satisfy the electricity loads. The planning model is tested in a variety of areas with diverse climate conditions, and the results are also compared in terms of levelized cost of energy. The numerical experiments show that net-zero energy operation is cost-effective in areas where the WT capacity factor is above 0.25 or the PV capacity factor reaches 0.45. Sensitivity analyses show that, if the battery cost is \$0.1-0.5M/MWh, this technology is not competitive in high wind profile area, yet PV coupled with battery system is always preferred despite the current high battery cost. Results also show that a grid-connected microgrid with net metering yields lower levelized cost of energy than an island microgrid.

The paper contributes to the modeling and application of microgrid integration in industrial systems for attaining eco-friendly operations. In modeling, we develop a climate analytics method to characterize

Table 9Transpiration distance and cost of factory and warehouse.

Factory ID.	Factory Location	Warehouse Phoenix (km)	Austin (km)	Product A Phoenix (\$/item)	Austin (\$/item)	Product B Phoenix (\$/item)	Austin (\$/item)
1	Yuma	298	1808	14	85	19	115
2	El Paso	693	923	33	43	44	59
1	San Francisco	1204	2814	57	132	77	179
2	Dallas	1710	312	80	15	109	20

wind and solar capacity factors based on 11-year, 64,240 meteorological records. For applications, the proposed two-stage planning model potentially accelerates the organizations to transition toward an "energy prosumer" who can actively participate in energy market as a consumer and a supplier. As the future effort, the model will be expanded to accommodate more stakeholders including retailers. The current numerical experiment is built upon a wafer fabrication process. Other manufacturing sectors, such as automobiles, oil refinery, and air-separation, will be considered for further examining and comparing the

model performance.

Acknowledgment

This project is partly supported by the National Science Foundation (NSF) under CBET Grant No. 1704933. The second author also wannts to thank the constructive comments received from the faculty of Dongwu Business School at Soochow University, China when this research was originally presented there in June 2018.

Appendix A. Estimating WT and PV Capacity Factor

A.1. Wind Turbine Capacity Factor

A WT system possesses four operating phases depending on the wind speed ν . Let $P_w(\nu)$ be the instantaneous power output of a turbine at speed ν . Then the cubic power curve is given as (Thiringer and Linders, 1993).

$$P_{w}(v) = \begin{cases} 0 & v < v_{c}, \quad v > v_{s} \\ P_{m}(v/v_{r})^{3} & v_{c} \leq v \leq v_{r} \\ P_{m} & v_{r} \leq v \leq v_{s} \end{cases}$$
(A1)

where v_c , v_r and v_s stand for the cut-in, rated, and cut-off wind speed, respectively. Note P_m is the rated power capacity. For wind speed fitting to a Weibull distribution, the probability density function and the cumulative distribution function are given below

$$f_w(v) = \frac{k}{c} (\frac{v}{c})^{k-1} e^{-(v/c)^k}, \text{ for } v \ge 0$$
 (A2)

$$F_w(v) = e^{-(v/c)^k}, \text{ for } v \ge 0$$
(A3)

where c and k are the scale and shape parameter, respectively. Then the WT capacity factor, denoted as λ_w is

$$\lambda_{w} = \frac{E[P_{w}(V)] \times T}{P_{m} \times T} = \frac{1}{v_{r}^{3}} \int_{v_{c}}^{v_{r}} v^{3} f_{w}(v) dv + (F_{w}(v_{s}) - F_{w}(v_{r})), \tag{A4}$$

where T is the number of hours in a period. The value of λ_w falls in the range of [0, 1].

A.2. . PV Capacity Factor in the Northern Hemisphere

The output power of a PV system depends on multiple factors that are summarized in Table A1. Unless specified, the unit of all angles is radian (rad).

Table A1
Key parameters in PV power generation.

No.	Factor	Symbol	Explanation
1	weather coefficient	W_t	between 0 and 1
2	PV size (m ²)	A	PV surface area
3	PV efficiency	η	15-20% for commercial PV
4	calendar date	d	<i>d</i> ∈{1, 2,, 365}
5	solar hour (rad)	ω	related to the local hour
6	PV temperature (°C)	$T_{\mathbf{o}}$	operating temperature
7	latitude (rad)	Ø	depends on location
8	PV azimuth angle (rad)	α	if facing the south, $\alpha = 0$
9	PV tilt angle (rad)	β	between PV and the ground
10	Solar zenith angle (rad)	φ	between the zenith and Sun's ray
11	solar incident angle (rad)	θ	Between the norm to PV and Sun's ray
12	local hours	t	t = 1, 2,, 24

We present a three-step procedure to calculate the output power of a PV system based on the study of Cai et al. (2010). These steps are summarized as follows

Step 1. For PV facing the south, the sunrise and sunset times in day $d \in \{1, 2, ..., 365\}$ are given by

$$\cos(-\omega_{rise}) = \cos(\omega_{set}) = -\tan(\emptyset - \beta)\tan\delta,\tag{A5}$$

With

$$\delta = 0.40928 \sin(\frac{2\pi(d+284)}{365}),\tag{A6}$$

where, ω_{rise} and ω_{set} are, respectively, the sunrise and the sunset angles in day d perceived by the PV panel, and δ is the declination angle. PV has no power output before sunrise and after sunset.

Step 2. Estimating the solar irradiance incident on the PV at time t on date d under clear sky condition,

$$I_{t} = 1370(.0. \ 7^{(\cos \varnothing)^{-0.678}}) \left(1 + 0.034 \cos\left(\frac{2\pi(d-4)}{365}\right)\right) \left(\cos \theta + 0.1\left(1 - \frac{\beta}{\pi}\right)\right), \tag{A7}$$

where

$$\cos \emptyset = \cos \delta \cos \phi \cos \omega + \sin \delta \sin \emptyset, \tag{A8}$$

 $\cos \theta = \sin \delta \sin \varnothing \cos \beta - \sin \delta \cos \varnothing \sin \beta \cos \alpha + \cos \delta \cos \varnothing \cos \beta \cos \omega$

$$+\cos\delta\sin\varnothing\sin\beta\cos\omega\cos\alpha + \cos\delta\sin\beta\sin\omega\sin\alpha$$
 (A9)

In (A7) I_t is the solar irradiance (W/m²) received by the PV at time t of day d. The solar zenith angle φ is estimated by Equation (A8). The solar hour angle ω is determined by the local time t. Starting from $\omega = -\pi/2$ at 6am, It increases 15° every hour until reaching $\omega = \pi/2$ at 6pm. To maximize the energy yield, the PV panel faces the South and its tilt angle shall equal the local latitude, namely if $\alpha = 0$ and $\beta = \phi$, then equation (A9) can be simplified as

$$\cos \theta = \cos \delta \cos \omega \tag{A10}$$

Step 3. The actual output of a PV system with the uncertain weather condition now can be estimated as

$$P_t = W_t \eta A I_t [1 - 0.005(T_0 - 25)], \tag{A11}$$

where P_t is the actual output power (in Watt) of the PV system. W_t is a weather coefficient that varies from 1 to 0 to mimic the nine states of the weather condition (Lave and Kleissl, 2011). The values of W_t are summarized in Table A2. The capacity factor of a PV system can be estimated by

$$\lambda_{PV} = \frac{1}{P_{PV}^{\text{max}} \times T} \sum_{t=1}^{T} P_t \tag{A12}$$

where P_{PV}^{\max} is the rated capacity of a PV system, and T is the number of generation hours. For PV in the Southern Hemisphere, simply set $\alpha = \pi$ and change ϕ into a native angle.

Table A2
Weather Coefficients under Different States

No.	1	2	3	4	5	6	7	8	9
State	Clear Sky	SC	PC	MC	Overcast	Rain	Fog	Storm	Snow
W_t	1	0.7	0.5	0.3	0.2	0.1	0.1	0.1	0

Appendix B. Labor and Machine Resources Available

Table B1 Labor and Machine Hours for Cases 1-5

Week	Labor (hour)	Machine (hour)	Week	Labor (hour)	Machine (hour)
1	38,516	278,847	27	37,860	279,542
2	34,429	244,299	28	39,153	281,016
3	33,472	239,044	29	32,345	237,514
4	34,210	248,699	30	34,562	249,292
5	36,680	261,478	31	36,814	263,851
6	36,660	269,935	32	35,001	251,627
7	34,063	249,447	33	32,159	239,152
8	35,786	261,961	34	37,138	269,049
9	36,243	261,441	35	36,784	267,032
10	36,989	268,359	36	30,487	223,362
11	33,739	240,138	37	31,639	226,421
12	35,560	263,343	38	28,497	208,141
13	36,920	262,138	39	33,601	241,714
14	37,695	268,946	40	33,727	249,509
15	33,051	240,437	41	35,735	259,884
16	38,113	276,789	42	32,750	237,912
17	33,914	241,252	43	35,657	257,745
18	33,569	243,591	44	32,635	240,033
19	38,010	274,606	45	34,452	249,525
20	37,688	270,170	46	33,684	244,778
21	40,853	291,900	47	37,094	267,545
22	38,946	283,740	48	30,751	226,419
23	28,867	215,059	49	38,739	270,781
24	34,891	248,255	50	34,252	250,829
25	31,466	230,446	51	40,363	292,169
26	30,652	219,114	52	32,078	230,129

Table B2
Labor and Machine Hours for Cases 6 and 7

	Labor		Machine	Machine		Labor	Labor		Machine	
Week	Factory 1	Factory 2	Factory 1	Factory 2		Factory 1	Factory 2	Factory 1	Factory 2	
1	22,339	16,177	153,366	125,481	27	21,959	15,901	153,748	125,794	
2	19,969	14,460	134,365	109,935	28	22,709	16,444	154,559	126,457	
3	19,414	14,058	131,474	107,570	29	18,760	13,585	130,633	106,881	
4	19,842	14,368	136,784	111,915	30	20,046	14,516	137,111	112,182	
5	21,275	15,406	143,813	117,665	31	21,352	15,462	145,118	118,733	
6	21,263	15,397	148,464	121,471	32	20,301	14,701	138,395	113,232	
7	19,757	14,306	137,196	112,251	33	18,652	13,507	131,533	107,618	
8	20,756	15,030	144,078	117,882	34	21,540	15,598	147,977	121,072	
9	21,021	15,222	143,793	117,648	35	21,335	15,449	146,868	120,165	
10	21,453	15,535	147,598	120,762	36	17,682	12,804	122,849	100,513	
11	19,568	14,170	132,076	108,062	37	18,351	13,288	124,532	101,890	
12	20,625	14,935	144,839	118,504	38	16,528	11,969	114,477	93,663	
13	21,413	15,506	144,176	117,962	39	19,488	14,112	132,943	108,771	
14	21,863	15,832	147,920	121,026	40	19,562	14,165	137,230	112,279	
15	19,170	13,881	132,241	108,197	41	20,726	15,009	142,936	116,948	
16	22,106	16,008	152,234	124,555	42	18,995	13,755	130,852	107,060	
17	19,670	14,244	132,688	108,563	43	20,681	14,976	141,760	115,985	
18	19,470	14,099	133,975	109,616	44	18,928	13,707	132,018	108,015	
19	22,046	13,303	151,033	123,573	45	19,982	14,470	137,239	112,286	
20	21,859	15,829	148,593	121,576	46	19,536	14,147	134,628	110,150	
21	23,695	17,158	160,545	131,355	47	21,515	15,580	147,150	120,395	
22	22,589	16,357	156,057	127,683	48	17,836	12,915	124,530	101,889	
23	16,743	12,124	118,283	96,777	49	22,469	16,270	148,930	121,852	
24	20,237	14,654	136,540	111,715	50	19,866	14,386	137,956	112,873	
25	18,250	13,216	126,745	103,701	51	23,410	14,127	160,693	131,476	
26	17,778	12,874	120,513	98,601	52	18,605	13,473	126,571	103,558	

References

Blackadar, A.K., Tennekes, H., 1968. Asymptotic similarity in neutral, barotropic, atmospheric boundary layers. J. Atmos. Sci. 25 (11), 1015–1020.

Bolinger, M., Weaver, S., Zuboy, J., 2015. "Is \$50/MWh solar for real? Falling project prices and rising capacity factors drive utility-scale PV toward economic competitiveness. Prog. Photovoltaics Res. Appl. 23 (12), 1847–1856.

Bouchery, Y., Ghaffari, A., Jemai, Z., Dallery, Y., 2012. Including sustainability criteria into inventory models. Eur. J. Oper. Res. 222 (2), 229–240.

Cai, T., Duan, S., Chen, C., 2010. Forecasting power output for photovoltaic grid-connected power systems without using solar radiation measurement. In: Proceedings of Power Electronics for Distributed Generation Systems Symposium, pp. 773–777.

Choi, Y.C., Xirouchakis, P., 2014. A production planning in highly automated manufacturing system considering multiple process plans with different energy requirements. Int. J. Adv. Manuf. Technol. 70 (5–8), 853–867.

Daclison-Dickey, R., 2013. "100 Electric Vehicles Begin Their Journey to Save 126,000 Gallons of Fuel Per Year," Longitudes, UPS. URL. http://blog.ups.com/2013/02/08/100-electric-vehicles-begin-theirjourney-to-save-126000-gallons-of-fuel-per-year/.

EV-Fleet, 2017. Condor electric truck specifications. available at. http://ev-fleet.com/ specifications/, Accessed date: 20 July 2017.

Federgruen, A., Zipkin, P., 1984. Approximation of dynamic, multi-location production and inventory problems. Manag. Sci. 30 (1), 69–84.

Freris, L., Infield, D., 2008. "Renewable Energy in Power Systems", Chapter 7. John Wiley & Sons, West Sussex, UK.

Golari, M., Fan, N., Jin, T., 2017. Multistage stochastic optimization for production-inventory planning with intermittent renewable energy. Prod. Oper. Manag. 26 (3), 409–425.

Golpira, H., Khan, S.A., Zhang, Y., 2018. Robust smart energy efficient production planning for a general job-shop manufacturing system under combined demand and supply uncertainty in the presence of grid-connected microgrid. J. Clean. Prod. 202 (11), 649–665.

Gong, X., Zhou, S.X., 2013. Optimal production planning with emissions trading. Oper. Res. 61 (4), 908–924.

Hart, D., Sarkissian, A., 2016. "Deployment of Grid Scale Batteries in the United States," Report of U.S. Department of Energy. available at. https://www.energy.gov/sites/prod/files/2017/01/f34, Accessed date: 11 May 2018.

Heier, S., 2005. Grid Integration of Wind Energy: Onshore and Offshore Conversion Systems, third ed. John Wiley & Sons, Chichester, UK, pp. 45.

Hickey, B., 2014. "Anheuser-Busch Brewing up Some Wind, Solar Power," KCRA News Archive, August 14, 2014. available at. http://www.kcra.com/article/anheuser-busch-brewing-up-some-wind-solar-power/6416039, Accessed date: 16 March 2017.

Higle, J.L., Kempf, K.G., 2010. Production planning under supply and demand uncertainty: a stochastic programming approach. In: In: Infanger, G. (Ed.), Stochastic

Programming. International Series in Operations Research & Management Science, vol. 150. Springer, New York, NY, pp. 297–315.

Hu, S., Souza, G.C., Ferguson, M.E., Wang, W., 2015. Capacity investment in renewable energy technology with supply intermittency: data granularity matters!. Manuf. Serv. Oper. Manag. 17 (4), 480–494.

Hua, G., Cheng, T.C.E., Wang, S., 2011. Managing carbon footprints in inventory management. Int. J. Prod. Econ. 132 (2), 178–185.

Jin, T., Pham, A., Novoa, C., Temponi, C., 2017. A net-zero carbon supply chain model: minimizing levelized cost of onsite renewable generation. Supply Chain Forum Int. J. 18 (2), 49–59.

Karki, R., Hu, P., Billinton, R., 2006. A simplified wind power generation model for reliability evaluation. IEEE Trans. Energy Convers. 21 (2), 533–540.

Lave, M., Kleissl, J., 2011. Optimum fixed orientations and benefits of tracking for capturing solar radiation. Renew. Energy 36 (3), 1145–1152.

Lee, H.L., Yano, C.A., 1988. Production control in multistage systems with variable yield losses. Oper. Res. 36 (2), 269–279.

Letchford, C.W., Zachry, B.C., 2009. On wind, waves, and surface drag. In: Proceedings of the 5th European and African Conference on Wind Engineering Conference, July 19-23, pp. 1–32.

Li, B., Tian, Y., Chen, F., Jin, T., 2017. Toward net-zero carbon manufacturing operations: an onsite renewables solution. J. Oper. Res. Soc. 68 (3), 308–321.

Masmoudi, O., Yalaoui, A., Ouazene, Y., Chehade, H., 2017. Lot-sizing in a multi-stage flow line production system with energy consideration. Int. J. Prod. Res. 55 (6), 1640–1663.

McMahon, J., 2011. Achieving net-zero use of grid energy in manufacturing—OPEX. North American Clean Energy available at. https://www.opex.com/articles-case-studies/achieving-net-zero-use-of-grid-energy-in-manufacturing, Accessed date: 23 May 2017.

Megahed, A., Goetschalckx, M., 2018. Tactical supply chain planning under uncertainty with an application in the wind turbines industry. Comput. Oper. Res. 100 (December issue), 287–300.

Mula, J., Poler, R., Garca-Sabater, J.P., Lario, F.C., 2006. Models for production planning under uncertainty: a review. Int. J. Prod. Econ. 103 (1), 271–285.

NREL, 2013. "Distributed Generation Renewable Energy Estimate of Costs," National Renewable Energy Laboratory Report. Available at. http://www.nrel.gov/analysis/tech_lcoe_re_cost_est.html, Accessed date: 7 May 2015.

Pechmann, A., Schöler, I., Ernst, S., 2016. Possibilities for CO 2-neutral manufacturing with attractive energy costs. J. Clean. Prod. 138, 287–297.

Pless, S., Torcellini, P., 2010. Net-zero energy buildings: a classification system based on renewable energy supply options. Nat. Renew. Energy Lab. Rep. http://netzerofoun, dation.org/docs/NREL, Accessed date: 3 March 2017.

Sox, C.R., Muckstadt, J.A., 1996. Multi-item, multi-period production planning with uncertain demand. IIE Trans. 28 (11), 891–900.

Thiringer, T., Linders, J., 1993. Control by variable rotor speed of a fixed pitch wind

- turbine operating in a wide speed range. IEEE Trans. Energy Convers. 8 (3), 520–526. Vallee, F., Lobry, J., Deblecker, O., 2007. Impact of the wind geographical correlation level for reliability studies. IEEE Trans. Power Syst. 22 (4), 2232–2239.
- Weekes, S.M., Tomlin, A.S., 2014. Comparison between the bivariate Weibull probability approach and linear regression for assessment of the long-term wind energy resource using MCP. Renew. Energy 68 (8), 529–539.
- WU (Weather Underground), 2017. Available at. http://www.wunderground.com/, Accessed date: 2 February 2017.
- Yano, C.A., Lee, H.L., 1995. Lot sizing with random yields: a review. Oper. Res. 43 (2), 311–334
- Zhang, M., Küçükyavuz, S., Yaman, H., 2012. A polyhedral study of multiechelon lot sizing with intermediate demands. Oper. Res. 60 (4), 918–935.
- Zhang, W., Hua, Z., Xia, Y., Huo, B., 2016. Dynamic multi-technology production-inventory problem with emissions trading. IIE Trans. 48 (2), 110–119.
- Zhang, H., Cai, J., Fang, K., Zhao, F., W. Sutherland, J., 2017. Operational optimization of a grid-connected factory with onsite photovoltaic and battery storage systems. Appl. Energy 205 (11), 1538–1547.
- Zhang, Y., Islam, M.M., Sun, Z., Yang, S., Dagli, C., Xiong, H., 2018. Optimal sizing and planning of onsite generation system for manufacturing in Critical Peaking Pricing demand response program. Int. J. Prod. Econ. 206, 261–267 December Issue.